

Quasi-particle spectrum and entanglement generation after a quantum quench in the quantum Potts spin chain

O. Pomponio¹, L. Pristyák¹ and G. Takács^{1,2*}

¹*BME Department of Theoretical Physics, H-1117 Budapest, Budafoki út 8.*

²*BME “Momentum” Statistical Field Theory Research Group, H-1117 Budapest, Budafoki út 8.*

(Dated: 10th October 2018)

Recently, a non-trivial relation between the quasi-particle spectrum and entanglement entropy production was discovered in non-integrable quenches in the paramagnetic Ising quantum spin chain. Here we study the dynamics of analogous quenches in the quantum Potts spin chain. Tuning the parameters of the system, we observe a sudden increase in the entanglement production rate, which is shown to be related to the appearance of new quasiparticle excitations in the post-quench spectrum. Our results demonstrate the generality of the effect and support its interpretation as the non-equilibrium version of the well-known Gibbs paradox related to mixing entropy which appears in systems with a non-trivial quasi-particle spectrum.

I. INTRODUCTION

A paradigmatic protocol for taking a quantum many-body system out of equilibrium is provided by a quantum quench, which corresponds to sudden change in the Hamiltonian. It is a protocol routinely engineered in cold-atom experiments [1–9] and provides a fruitful starting point to study non-equilibrium time evolution of isolated quantum systems. When both the pre- and post-quench Hamiltonians are translationally invariant, a quench starting from an equilibrium (e.g. ground) state of the pre-quench system corresponds to a situation with a uniform non-zero energy density under the post-quench Hamiltonian, which is a highly excited configuration that can be considered as a source of quasi-particle excitations [10]. The subsequent time evolution can be considered as dynamics driven by the quasi-particles created in the quench; the post-quench excitations determine the spreading of correlation and entanglement in the system.

Entanglement entropy is an important characteristics of the non-equilibrium evolution and the stationary state resulting after a quench, and therefore it has been studied extensively in recent years [13–26]. The growth of entanglement also has important implications for the efficiency of computer simulations of the time evolution [27–30]. Recently it has become possible to measure entanglement entropy and its temporal evolution in condensed matter systems [2, 31, 32].

For systems where interactions have a suitable fall-off with distance, the quasi-particle propagation is limited by the existence of a maximum speed v_{\max} called the Lieb–Robinson bound [11]. For the entanglement entropy S_ℓ of a subsystem of length ℓ with the rest of system this results in an overall linear growth of entanglement entropy $S_\ell(t) \sim t$ for times $t < \ell/2v_{\max}$, after which it becomes saturated as the subsystem approaches its stationary state [12]. The late time asymptotic value of entanglement entropy of a large subsystem can also be in-

terpreted as the usual thermodynamic entropy [2, 12, 33–35].

In the regime dominated by the linear growth, entanglement generation can be characterised by the mean entanglement entropy production rate $\overline{\partial_t S}$, which naturally depends on the post-quench spectrum and its quasi-particle content. For quenches to integrable systems entanglement dynamics be computed from a recently developed approach [33, 36–38]. The underlying quasi-particle description of entropy production describes the initial state as a source of entangled quasi-particle pairs with zero total momentum [10] the members of which propagate to different parts of the system, resulting in the build-up of spatial correlations and entanglement growth. This picture was explicitly demonstrated for integrable quenches in the Ising spin chain [39] and also forms the basis of a semi-classical approach for quantum quenches [40], which is expected to be valid for sufficiently small post-quench density even in the non-integrable case. It also successfully describes entropy production in integrable systems [33, 37] and leads to the following formula for the late time growth of the entanglement entropy of a subsystem of size ℓ [12, 33, 37]:

$$S(t) \propto 2t \sum_n \int_{2v_n t < \ell} dk v_n(k) f_n(k) + \ell \sum_n \int_{2v_n t > \ell} dk f_n(k) , \quad (I.1)$$

where n enumerates the different quasi-particle species, k is the momentum of the quasi-particles, $v_n(k)$ is their velocity and $f_n(k)$ is a rate function describing the entropy produced by quasi-particle pairs of species n which depends on their production rate. The restriction in the integrals reflects light-cone propagation as a consequence of the Lieb–Robinson bound. For entanglement entropy between two halves of an infinite system $\ell = \infty$, and so the second term describing saturation is absent, while the integral in the first one has no restriction so Eq. (I.1) simplifies to

$$S(t) \propto 2t \sum_n \int dk v_n(k) f_n(k) . \quad (I.2)$$

* Corresponding author (email: takacsg@eik.bme.hu)

For free systems, the computation can be extended to a more general class of initial states containing non-pair configurations [41]. More recently, the generalised hydrodynamics approach to inhomogeneous quenches [42, 43] was applied to compute entanglement in free [44] and integrable [45] systems.

Much less is known about entanglement dynamics in quenches governed by non-integrable post-quench dynamics. In the case of the quantum Ising chain it was shown in recent studies that switching on an integrability breaking longitudinal magnetic field h_x leads to non-trivial dynamical phenomena. In the ferromagnetic regime confinement suppresses the usual linear growth of entanglement entropy and the corresponding light-cone-like spreading of correlations after the quantum quench [46]. In contrast, there is no confinement in the paramagnetic regime and thus entanglement entropy grows linearly in time. Nevertheless the dependence of the mean entanglement entropy production rate $\overline{\partial_t S}$ on the quench parameter h_x shows another kind of anomalous behaviour: a sudden increase setting at the threshold value of h_x where a new quasi-particle excitation appears in the spectrum [47]. Using the physical interpretation of the asymptotic entanglement of a large subsystem as the thermodynamic entropy of the stationary (equilibrium) state, this can be recognised as arising from the contribution of mixing entropy between the particle species, and so the effect can be interpreted as a non-equilibrium manifestation of the Gibbs paradox.

The purpose of the present work is to demonstrate the same mechanism in the quantum Potts spin chain, which is a generalisation of the Ising case with three instead of two values for the spin variables. Due to the higher symmetry of the chain, its spectrum and behaviour is much richer, and a full exploration of the parameter space is out of the scope of the present work. Instead we focus on the non-equilibrium manifestation of the Gibbs mixing entropy analogous to the effect found in [47] to show that it generalises to the Potts chain, and to support the interpretation advanced in [47].

The outline of the paper is as follows. Quenches in the paramagnetic phase are considered first in Section II, where it is shown that the effect observed in [47] generalises from the Ising to the Potts case. The determination and analysis of spectrum in the paramagnetic phase are presented in Section III. Section IV analyses the relation between the time evolution and the quasi-particle spectrum, arguing that the scenario proposed in [47] holds for the Potts case as well, and also discussing specific aspects where the Potts model differs from the Ising case considered in [47]. Section V contains our conclusions.

II. QUENCHES IN THE QUANTUM POTTS SPIN CHAIN

The 3-state Potts quantum spin chain is defined on the Hilbert space

$$\mathcal{H} = \bigotimes_{i=1}^L (\mathbb{C}^3)_i \quad (\text{II.1})$$

where i labels the sites of the chain of length L . The quantum space \mathbb{C}^3 at site i has the basis $|\alpha\rangle$ with $\alpha = 0, 1, 2$ corresponding to the spin degrees of freedom. The dynamics is defined by the Hamiltonian

$$H = -J \sum_{i=1}^L \left[\sum_{\alpha=0}^2 (P_i^\alpha P_{i+1}^\alpha + h_\alpha P_i^\alpha) + g \tilde{P}_i \right] \quad (\text{II.2})$$

where

$$P^\alpha = |\alpha\rangle\langle\alpha| - \frac{1}{3} \mathbf{1}_{3\times 3} \quad (\text{II.3})$$

$$\tilde{P} = \frac{1}{3} \sum_{\alpha, \alpha'=0}^2 (1 - \delta_{\alpha\alpha'}) |\alpha\rangle\langle\alpha'|$$

and we assume periodic boundary conditions

$$P_{L+1}^\alpha \equiv P_1^\alpha, \quad \tilde{P}_{L+1} \equiv \tilde{P}_1 \quad (\text{II.4})$$

The parameters h_α and g are dimensionless, while energy (and by implication, time) units are specified by J . In all of our subsequent numerical calculations we use units with $J = 1$ and also $\hbar = 1$.

In the absence of the “longitudinal” magnetic fields h_α , the chain is invariant under the \mathbb{S}_3 permutation symmetry of the three spin states $\alpha = 0, 1, 2$ and it has a critical point at $g = 1$ corresponding to a phase transition between a paramagnetic (PM) $g > 1$ and ferromagnetic (FM) $g < 1$ case. In the PM phase, there is a single \mathbb{S}_3 invariant vacuum, while in the FM phase there are three vacua that become degenerate in the infinite length limit. The order parameter for the transition is given by the magnetizations $m^{(\alpha)} = \langle P_i^\alpha \rangle$ and the quantum critical point separating the phases can be described with a conformal field theory (CFT) with central charge $c = 4/5$.

A. The quench protocol and the simulation procedure

The non-equilibrium time evolution we study is defined by the following quench protocol. The initial state is the ground state $|\Psi(0)\rangle$ of the pre-quench Hamiltonian

$$H_{\text{pre}} = -J \sum_{i=1}^L \left[\sum_{\alpha=0}^2 (P_i^\alpha P_{i+1}^\alpha) + g \tilde{P}_i \right] \quad (\text{II.5})$$

which is unique in the paramagnetic phase $g > 1$. We consider four values $g = 1.25, 1.5, 1.75$ and 2.0 , and the time evolution is given by

$$|\Psi(t)\rangle = e^{-iHt} |\Psi(0)\rangle$$

where the post-quench Hamiltonian is given by (III.4):

$$H = -J \sum_{i=1}^L \left(\sum_{\alpha=0}^2 P_i^\alpha P_{i+1}^\alpha + h P_i^0 + g \tilde{P}_i \right) \quad (\text{II.6})$$

and we consider the time evolution as a function of h which is taken to be non-negative.

The time evolution is computed using the infinite volume time evolving block decimation (iTEBD) algorithm [48]. Using translational invariance, the many-body state is represented as the Matrix Product State (MPS)

$$|\Psi\rangle = \sum_{\dots, s_j, s_{j+1}, \dots} \dots \Lambda_o \Gamma_o^{s_j} \Lambda_e \Gamma_e^{s_{j+1}} \dots | \dots, s_j, s_{j+1}, \dots \rangle,$$

where s_j spans the local 3-dimensional spin Hilbert space, $\Gamma_{o/e}^s$ are $\chi \times \chi$ matrices associated with the odd/even lattice site; $\Lambda_{o/e}$ are diagonal $\chi \times \chi$ matrices with the singular values corresponding to the bipartition of the system at the odd/even bond as their entries. The many-body state is initialised to the product state $|\Psi_0\rangle = \bigotimes \frac{1}{\sqrt{3}} (|0\rangle + |1\rangle + |2\rangle)$. The ground state $|\Psi(0)\rangle$ was obtained by time-evolving the initial state $|\Psi_0\rangle$ in imaginary time by the pre-quench Hamiltonian (II.5), using a second-order Suzuki-Trotter decomposition of the evolution operator with imaginary time Trotter step $\tau = 10^{-3}$. Due to the presence of an energy gap, an auxiliary dimension $\chi_0 = 81$ was sufficient to have a very accurate result for the ground state.

The post-quench time evolution was obtained by evolving $|\Psi(0)\rangle$ with the post-quench Hamiltonian (II.6) in real time, again using a second-order Suzuki-Trotter decomposition of the evolution operator with real time Trotter step $\delta t = 0.005$. To keep the truncation error small the auxiliary dimension was allowed to grow up to $\chi_{\max} = 243$ which was sufficient to reach a maximum time $T = 40$.

B. Entanglement growth rate

The central issue of this work concerns the evolution of the half-system entanglement entropy $S(t)$. This is defined by cutting the system into two halves \mathcal{H} and $\bar{\mathcal{H}}$ and introducing the reduced density matrix

$$\rho_{\mathcal{H}}(t) = \text{Tr}_{\bar{\mathcal{H}}} |\Psi(t)\rangle \langle \Psi(t)|$$

Then the half-system entanglement entropy is given by

$$S(t) = -\text{Tr}_{\mathcal{H}} \rho_{\mathcal{H}}(t) \log \rho_{\mathcal{H}}(t).$$

As illustrated in Fig. II.1 after a relatively short transient $S(t)$ shows a linear trend (with some slowly decaying oscillations) as expected after a global quantum quench. A numerical estimation of the mean entanglement entropy production rate $\overline{\partial_t S}$ was obtained by a linear fit of

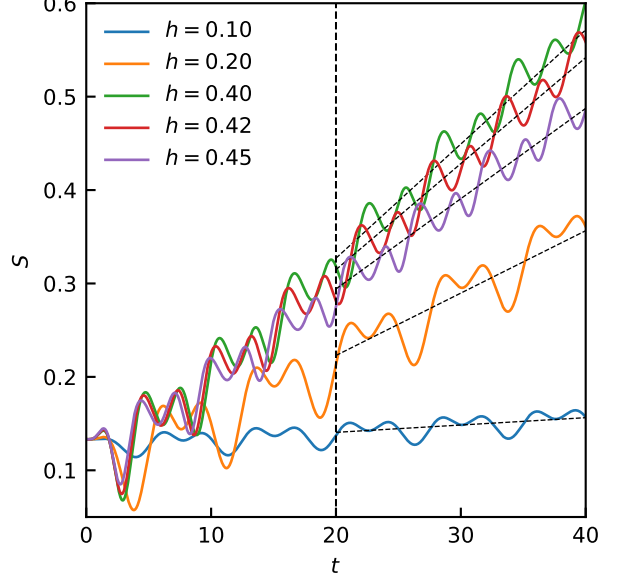


Figure II.1: The time evolution of $S(t)$ for $g = 1.75$ and $h = 0.10, 0.20, 0.40, 0.42$ and 0.45 , where time is measured in units of $1/J$. The vertical line drawn at time t shows the limit above which the average slope was extracted, the corresponding fits are shown by the black dotted lines.

the iTEBD data in the time window $20 \leq t \leq 40$. The dependence of $\overline{\partial_t S}$ on h for the values of the transverse field $g = 1.25, 1.5, 1.75$ and 2.0 is shown in Fig. II.2. It can be seen clearly that $\overline{\partial_t S}$ has a local minimum at a value h_{\min} , the values of which are summarised in the following table:

g	1.25	1.5	1.75	2.0
h_{\min}	0.10	0.28	0.49	0.72

This very peculiar, non-monotonous behaviour of $\overline{\partial_t S}$ was previously seen for quenches in the paramagnetic Ising spin chain [47] where it was explained by the effect of the quasi-particle spectrum on the entanglement entropy production. In the following we investigate the detailed dynamics of the Potts model to see whether it confirms the scenario proposed in [47], which posited that the reversal of the decreasing trend in $\overline{\partial_t S}$ at h_{\min} is due to the appearance of a new quasi-particle excitation in the spectrum, which enhances entropy production by increasing the number of species available.

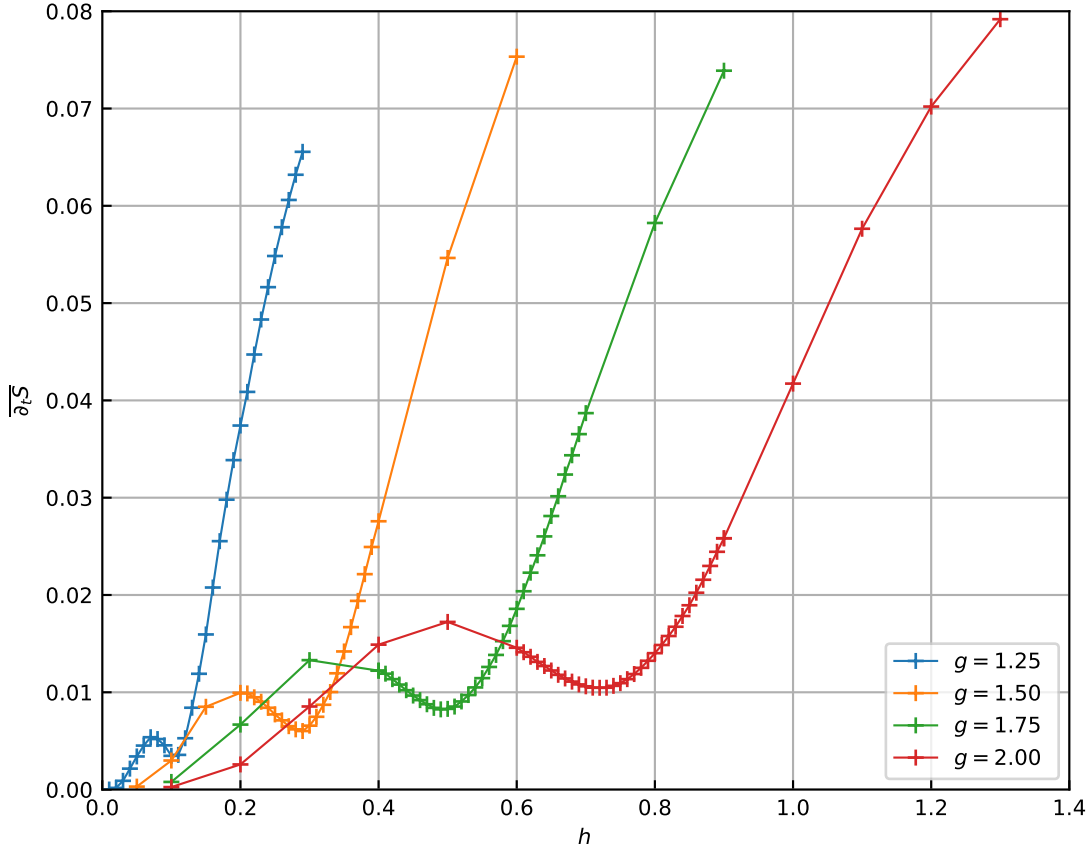


Figure II.2: The mean entanglement entropy production rate $\overline{\partial_t S}$ as a function of h for $g = 1.25, 1.5, 1.75$ and 2.0 .

III. SPECTRUM OF THE PARAMAGNETIC POTTS SPIN CHAIN

A. The case $h_\alpha = 0$

In the ferromagnetic phase the quasi-particle spectrum of the chain consists of kink excitations $K_{\alpha\beta}$ connecting the vacua according to the adjacency condition

$$\alpha - \beta = \pm 1 \bmod 3 \quad (\text{III.1})$$

with an obvious action of the permutation symmetry.

In the paramagnetic phase the quasi-particle spectrum consists of doubly degenerate magnons. Choosing two generators \mathcal{C} and \mathcal{T} for the group \mathbb{S}_3 which satisfy the relations

$$\mathcal{T}^3 = 1 \quad , \quad \mathcal{C}^2 = 1 \quad , \quad \mathcal{C}\mathcal{T}\mathcal{C} = \mathcal{T}^{-1} \quad (\text{III.2})$$

one can introduce a basis in the magnonic space with one-particle states at fixed momentum given by $|A(k)\rangle$ and $|\bar{A}(k)\rangle$. They form the two-dimensional irreducible rep-

resentation of \mathbb{S}_3 defined by the relations:

$$\begin{aligned} \mathcal{T}|A(k)\rangle &= e^{2\pi i/3}|A(k)\rangle \\ \mathcal{T}|\bar{A}(k)\rangle &= e^{-2\pi i/3}|\bar{A}(k)\rangle \\ \mathcal{C}|A(k)\rangle &= |\bar{A}(k)\rangle \end{aligned} \quad (\text{III.3})$$

For more information regarding the quasi-particle spectrum of the chain we refer the interested reader to the work [49] and references therein.

B. The case $h_\alpha \neq 0$

Switching on one or more longitudinal magnetic fields h_α leads to an explicit breaking of the symmetry group \mathbb{S}_3 . In the ferromagnetic case this results in confinement which is well-studied in the scaling limit [50–54]. However, in this work we are interested in the paramagnetic phase, and consider switching on one of the fields $h_0 = h \neq 0$ and keeping $h_{1,2} = 0$. Therefore our Hamiltonian is

$$H = -J \sum_{i=1}^L \left(\sum_{\alpha=0}^2 P_i^\alpha P_{i+1}^\alpha + h P_i^0 + g \tilde{P}_i \right) \quad (\text{III.4})$$

This partially breaks the symmetry \mathbb{S}_3 , leaving only a \mathbb{Z}_2 subgroup intact. We choose the generator \mathcal{C} to correspond to the unbroken subgroup, which in this case is generated by the transformation swapping the spin directions 1 and 2. Then for $h = 0$ one can introduce the quasi-particle basis corresponding to the eigenstates of \mathcal{C}

$$|A_{\pm}(k)\rangle = \frac{1}{\sqrt{2}} (|A(k)\rangle \pm |\bar{A}(k)\rangle) \quad (\text{III.5})$$

For $h = 0$ they are degenerate, but for a non-zero h the degeneracy is lifted. As shown below, similarly to the case of the Ising spin chain [47], for any fixed $g > 1$ there is some critical value h_{crit} above which two A_+ quasi-particles form a \mathcal{C} -even bound state B which can formally be written as a two-particle state with imaginary relative momentum

$$|B(k)\rangle \propto |A_+(k/2 + i\kappa/2)A_+(k/2 - i\kappa/2)\rangle. \quad (\text{III.6})$$

It is likely that the spectrum shows a larger variation when considering the whole range of parameters h_{α} and g (in the Ising case, there also exist another bound state for larger values of h : cf. [47] for the spin chain, and [57] for the scaling field theory). However, in this work we restrict ourselves to the regions $0 \leq h \leq h_{\text{crit}}$ and $h_{\text{crit}} \lesssim h$, and leave a more complete exploration of the parameter space for the future.

C. Quasi-particle dispersion relations for $h > 0$

We determined the quasi-particle dispersion relations applying exact diagonalisation of the Hamiltonian (III.4). After determining a few hundred states at the bottom of the spectrum, they were sorted into bins containing energy levels that are degenerate within numerical precision. Most of the eigenvalues appear in degenerate pairs of states with opposite total momentum k and $-k$, with the exception of singlets with momenta $k = 0$ and $k = \pi$. Momenta of states can be obtained by diagonalising the shift operator \mathcal{S} mapping site i to site $i+1 \bmod L$ within the bins. In the paramagnetic phase, the ground state is an isolated singlet, followed by two branches of one particle states corresponding to momenta

$$k_n = n \frac{2\pi}{L}, \quad n = \left[-\frac{L}{2} \right] + 1, \dots, \left[\frac{L}{2} \right] \quad (\text{III.7})$$

where the two branches are distinguished by the eigenvalue of \mathcal{C} which corresponds to the unbroken \mathbb{Z}_2 . We computed the quasi-particle branches for chain lengths L from 12 to 15. An example result is shown in Fig. III.1.

It turns out that dependence on the finite size L is very weak, so one can treat the results from different chain lengths L as sampling the same (infinite volume) dispersion relations $\epsilon_{\pm}(k)$. In addition, the fitting functions

$$\epsilon_{\pm}(k) = \sqrt{a_{\pm} + b_{\pm} \cos k} \quad (\text{III.8})$$

inspired by the free fermion dispersion relation provide an excellent description of the numerical data. The fits can be used to determine both the gaps

$$\Delta_{\pm} = \sqrt{a_{\pm} + b_{\pm}} \quad (\text{III.9})$$

and the Lieb-Robinson (LR) velocities

$$v_{\max \pm} = \max_k \frac{\partial \epsilon_{\pm}}{\partial k} \quad (\text{III.10})$$

To find the bound state threshold, we use a different approach for the determination of the gap that leads to a much more precise result. Note that for each chain length one can obtain the value of the gap $\Delta_{\pm}(L)$ from the energy of the first/second zero momentum excited state relative to the ground state. Using the theory of finite size effects [55] one can then extrapolate these to infinite volume using the fitting functions

$$\Delta_{\pm}(L) = \Delta_{\pm} + \gamma_{\pm} e^{-\mu_{\pm} L} \quad (\text{III.11})$$

For the choices of the transverse field $g = 1.25, 1.5, 1.75$ and 2.0 , the dependence of the gaps and LR velocities on the longitudinal field h are shown in Figs. III.2 and III.3, respectively.

D. Bound state threshold

1. Determination of h_{crit}

For $h < h_{\text{crit}}$, the part of the spectrum above the two quasi-particle branches consists of many-particle states called the continuum. Since $\Delta_+ < \Delta_-$ for $h > 0$, the lowest lying levels are two-particle states¹

$$|A_+(k/2 + q/2)A_+(k/2 - q/2)\rangle$$

of total momentum k taking the values (III.7), while q is their relative momentum, which is quantised differently due to interaction effects involving the scattering phase shift [56]. The lowest lying even state above $|A_+(0)\rangle$ corresponds to a zero-momentum state

$$|A_+(q_{\min}/2)A_+(-q_{\min}/2)\rangle$$

where q_{\min} is the smallest allowed value for the relative momentum q . When h approaches h_{crit} , q_{\min} goes to 0 and for $h > h_{\text{crit}}$ it turns imaginary according to the standard quantum mechanical relation between scattering and bound states, with the state becoming identical to

$$|B(0)\rangle$$

¹ In fact, this state can hybridize with A_-A_- two-particle states, but it does not change the subsequent considerations and so we omit this term for simplicity.

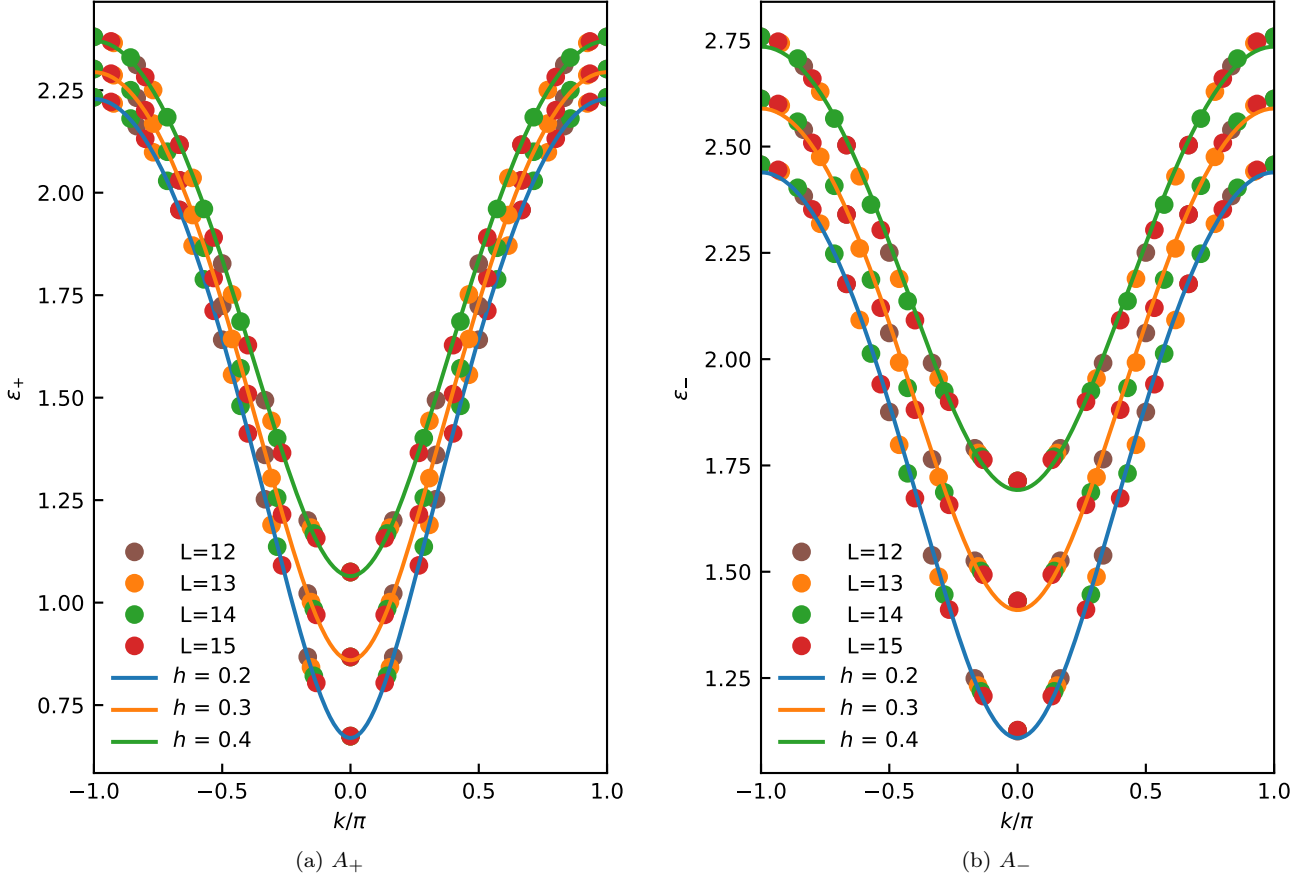


Figure III.1: Dispersion relations for A_+ and A_- for $g = 1.5$ and $h = 0.2, 0.3$ and 0.4 . Energies are shown in units of J , while momentum is shown in units of $1/a$, where a is the lattice spacing.

i.e. a zero-momentum level with a single B quasi-particle. Denoting the energy gap of this level by Δ_B one has

$$\begin{aligned} \Delta_B &> 2\Delta_+ & h < h_{\text{crit}} \\ \Delta_B &= 2\Delta_+ & h = h_{\text{crit}} \\ \Delta_B &< 2\Delta_+ & h > h_{\text{crit}} \end{aligned} \quad (\text{III.12})$$

which makes possible the determination of h_{crit} .

Finite size effects can be eliminated using the exponential extrapolation according to the leading order finite size dependence predicted in [55]

$$\Delta_B(L) = \Delta_B + \gamma_B e^{-\mu_B L} \quad (\text{III.13})$$

when $h > h_{\text{crit}}$. Here $1/\mu_B$ is a length scale corresponding to the spatial extension of the $A_+ A_+$ bound state wave function, which diverges at $h = h_{\text{crit}}$ and so the simple exponential extrapolation prescribed by (III.13) becomes impossible in the vicinity of the threshold h_{crit} , as illustrated in Fig. III.4. However, in that case γ_B vanishes as well since it corresponds to the effective coupling between two A_+ particles which changes sign from attractive to repulsive and so vanishes at the threshold,

so the finite volume dependence is much weaker as it is determined by subleading corrections.

For $h < h_{\text{crit}}$ the energy level is a scattering state and volume dependence is different (decaying as a power in L) and much better numerical data are necessary in order to describe it in terms of scattering characteristics [56]. However, since we are not interested in finding the actual value of the energy level in that range we can simply fit it by the same function (III.13) to keep our procedure uniform.

The value of h_{crit} can be determined by plotting Δ_B/Δ_+ as a function of h and finding the value where it crosses 2, as shown in Fig. III.5.

2. Dispersion relation for B

In the regime $h > h_{\text{crit}}$ the states with momenta (III.7) lying just above the two quasi-particle branches A_{\pm} correspond to single-quasi-particle states $|B(k_n)\rangle$, and their energies allow the determination of the dispersion relation of B as shown in Fig. III.6. Just as it was noted in the case of the Ising chain [47], the dispersion relation

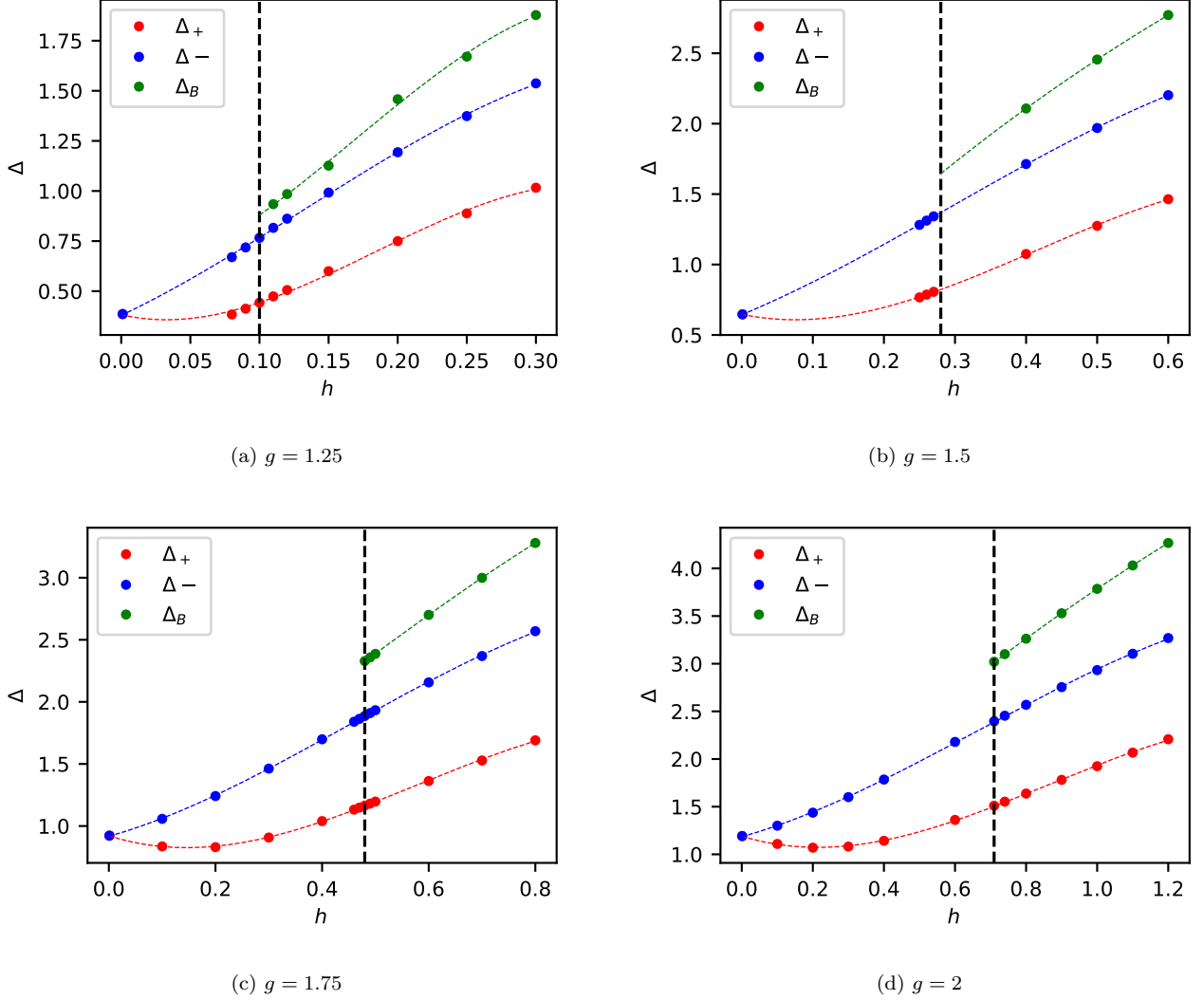


Figure III.2: Quasi-particle gaps Δ_{\pm} and Δ_B (in units of J) as functions of h . The vertical dashed line shows the threshold value of h above which the bound state quasi-particle B exists.

can be fitted well with the function

$$\epsilon_B(k) = \sqrt{a_B + b_B \cos k + c_B \cos 2k}$$

from which it is possible to determine both the gap $\Delta_B = \sqrt{a_B + b_B + c_B}$ and the Lieb-Robinson velocity $v_{\max\pm} = \max_k \frac{\partial \epsilon_{\pm}}{\partial k}$. Just as in the case of the “elementary” quasi-particles A_{\pm} , the gap Δ_B can also be determined using the extrapolation (III.13) which leads to a more accurate result. It is also clear from Fig. III.6 that moving closer to the threshold i.e. for smaller h , when the quasi-particle B becomes more weakly bound the finite size dependence becomes stronger, which is in fact expected from III.13 since when the spatial extension of the bound state wave function increases, the exponent μ_B becomes smaller.

IV. QUASI-PARTICLE SPECTRUM AND NON-EQUILIBRIUM TIME EVOLUTION

A. Time evolution of magnetisation

The three components of longitudinal magnetisation can be computed as

$$m_{\alpha}(t) = \langle \Psi(t) | P_i^{\alpha} | \Psi(t) \rangle$$

Due to translation invariance they are independent of the spatial position i and from the definitions (II.3) and the residual symmetry \mathbb{Z}_2 they satisfy

$$m_1(t) = m_2(t) = -\frac{m_0(t)}{2}.$$

Transverse magnetisation can be defined as

$$\tilde{m}(t) = \langle \Psi(t) | \tilde{P}_i | \Psi(t) \rangle.$$

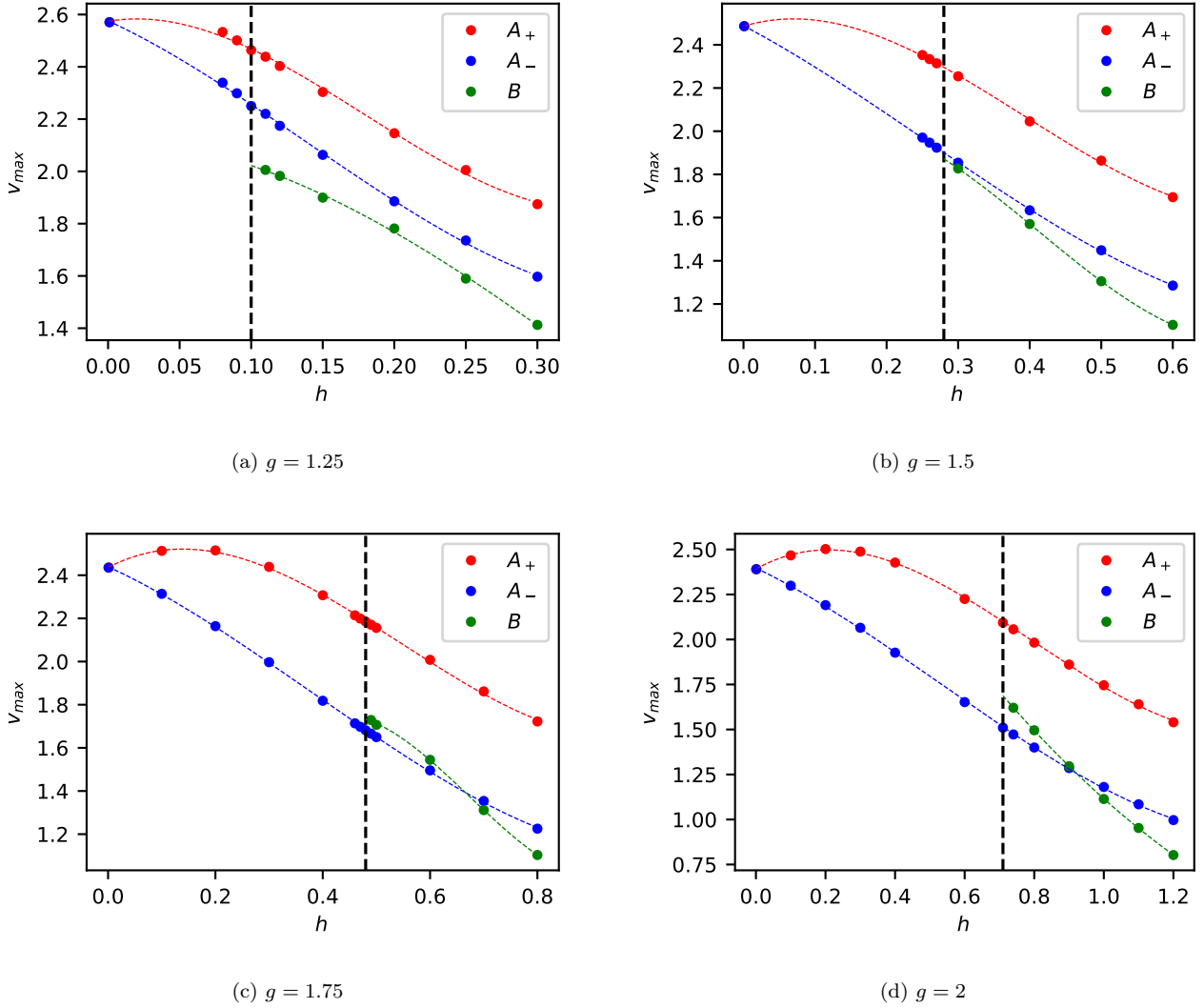


Figure III.3: Lieb-Robinson velocities $v_{\max\pm}$ and $v_{\max B}$ as functions of h . The vertical dashed line shows the threshold value of h above which the bound state quasi-particle B exists. Velocities are shown in units of Ja , where a is the lattice spacing.

An example of their time evolution is shown in Fig. IV.1. Following [46] and [47], the Fourier spectra of their time series can be used as to determine the post-quench quasi-particle spectrum via a sort of ‘‘quench spectroscopy’’. The power spectra were obtained using FFT with an angular frequency resolution $d\omega = 2\pi/T \simeq .157$ and are also illustrated in Figs. IV.1. They agree well with the predicted quasi-particle gaps; note that due to the \mathbb{Z}_2 symmetry of the initial state preserved by the post-quench Hamiltonian (II.6), only \mathcal{C} -even states are visible. The second peak in the power spectrum which appears above the critical value of h is the signature of a new bound state, in agreement with the predicted spectrum from exact diagonalisation.

We remark that the post-quench state has a finite energy density, which induces corrections in the quasi-

particle spectrum and introduces a finite life-time. The presence of well-defined quasi-particle peaks close to the values extracted from the spectrum of the zero-density system demonstrates that the post-quench dynamics can be described in terms of the quasi-particle picture despite the non-integrability of the system.

B. Time evolution of entanglement entropy

Now we return to the effect observed in Fig. II.2. Starting our discussion with the decreasing trend just before h_{\min} , we note that while presently a full quantitative understanding is missing, the qualitative picture is clear. The initial increase in $\partial_t S$ comes from the energy density of the quench increasing with h as shown in Fig.

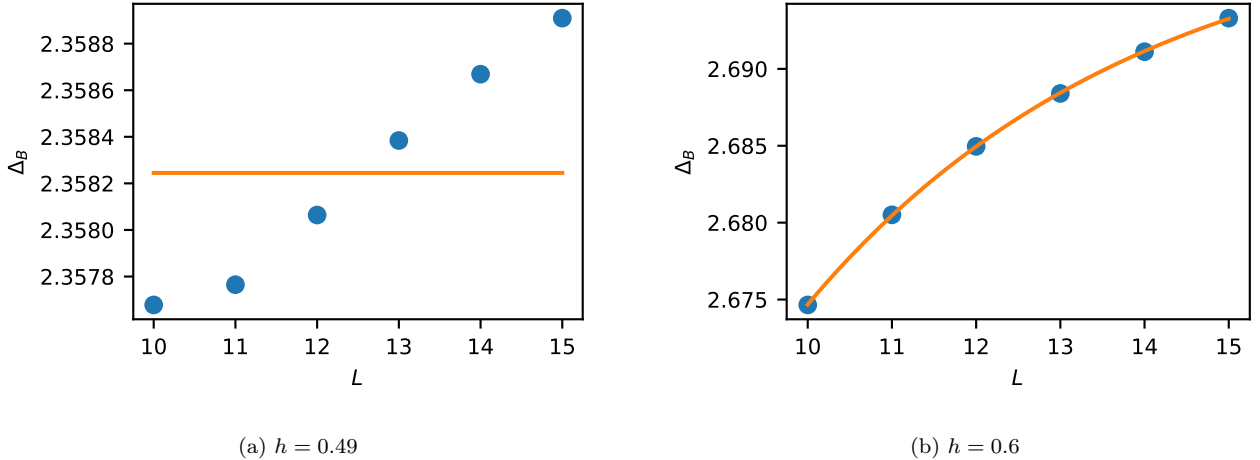


Figure III.4: Finite size extrapolation for the gap Δ_B (in units of J). Note that well above the threshold value of $h \approx 0.49$ the exponential fit works very well, while at the threshold it completely misses. However, the range of variation of Δ_B is much smaller when at the threshold, corresponding to the vanishing of the leading order finite size correction.

IV.2. The subsequent decline in $\overline{\partial_t S}$ is consistent with the quasi-particle gaps increasing, and the Lieb-Robinson velocities decreasing with h as demonstrated in Figs. III.2 and III.3, respectively. In fact for very large values of h the dynamics of the whole chain stops since the Potts spins are locked in the direction of h , suppressing the propagation of excitations along the chain as shown in the next Subsection.

Now let us consider the reversal of the decreasing trend, which happens at the position h_{\min} of the local minimum in $\overline{\partial_t S}$. The value of h_{\min} can be compared to the threshold h_{crit} for the excited even quasi-particle B :

g	1.25	1.5	1.75	2.0
h_{\min}	0.10	0.28	0.49	0.72
h_{crit}	0.10	0.28	0.48	0.71

It is clear that the two positions coincide within numerical accuracy (corresponding to the number of digits shown in the above table) for small values of g , while h_{\min} is slightly larger than h_{crit} for larger g . This is the same pattern as observed for the Ising spin chain in [47], and it can be explained in the same way.

Firstly, the appearance of the new quasi-particle species B for $h > h_{\text{crit}}$ leads to a steep increase in the entanglement entropy production due to the contribution of Gibbs mixing entropy arising from species information carried by the post-quench quasi-particles. While a full quantitative description is lacking at the moment, there is a simple argument using quasi-particle pair production rates determined in the scaling Ising field theory that shows that the presence of mixing entropy can lead to an order-of-magnitude increase in entropy production. This argument is detailed in the Supplementary Material of [47], and we do not repeat it here in detail.

Secondly, the fact that $h_{\min} - h_{\text{crit}}$ is non-zero and grows with g can also be easily understood. Note that before particle B appears, $\overline{\partial_t S}$ has a decreasing trend which is reversed by the appearance of B . However, the rate of production of pairs containing B is expected to rise only gradually. The reason is when B is only very weakly bound, the finite density post-quench medium easily destabilizes it. So the higher the value of h_{crit} , the larger is the quench when B appears, leading to a higher destabilizing effect of the post-quench medium to be overcome. Since h_{crit} increases with g , the difference $h_{\min} - h_{\text{crit}}$ is also expected to increase with g as well. This is indeed what was observed both here in the Potts case, and also the Ising case considered in [47].

C. Large h behaviour

Recalling the Hamiltonian (II.6) we see that for large $h \gg g$ the spins of the chain are essentially frozen in direction 0. This is consistent with the increasing gaps and decreasing velocities for the excitations shown in Figs. III.2 and III.3. For a very large value of h , the dynamics slows down and $\overline{\partial_t S}$ goes to zero, as shown in Fig. IV.3.

D. The regime $h < 0$

When $h < 0$, no freezing of the dynamics occurs for $h \ll -g$. The reason is that although a large negative h freezes direction 0, the energetically favoured directions 1 and 2 remain degenerate and so the chain effectively enters an Ising regime where $\overline{\partial_t S}$ grows monotonously with the amount of energy injected into the system

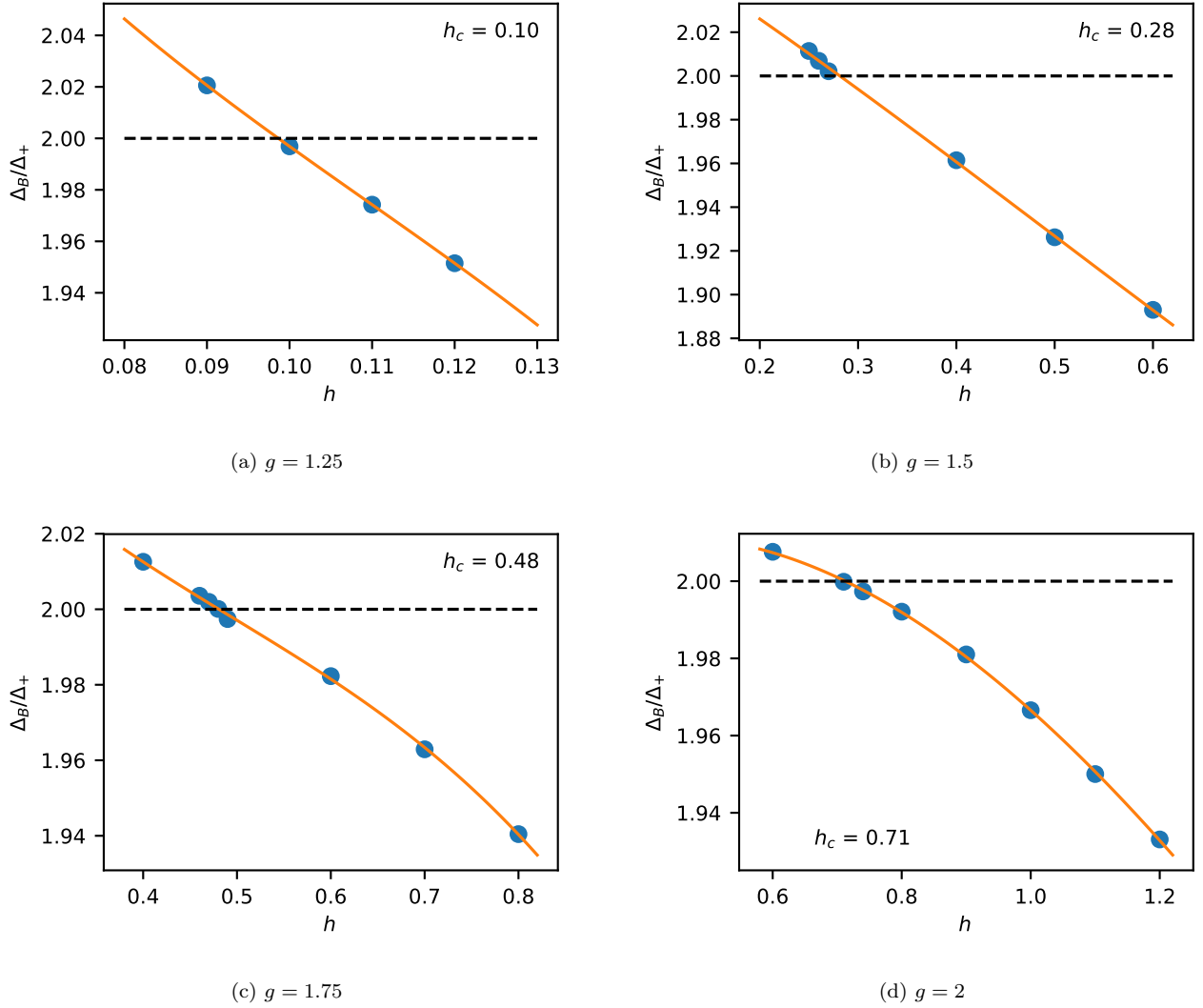


Figure III.5: Determining h_{crit} from Δ_B/Δ_+ as a function of h .

as shown in Fig. IV.4. Examining the quasi-particle threshold shows that here A_- is lighter than A_+ and there is even a threshold value h_- (≈ -0.19 for $g = 1.5$) below which $\Delta_+ > 2\Delta_-$. Therefore, for $h < h_-$ the excitation A_+ becomes unstable and decays into a pair of A_- particles and as a result, the number of available species therefore decreases.

Turning to the details of the quasi-particle spectrum, a direct calculation using exact diagonalisation (as described in Section III) shows that the quasi-particle gap Δ_- rapidly decreases, while the Lieb-Robinson velocities $v_{\max-}$ increases when h becomes more negative, as shown in Fig. IV.5. Coupled with the rapid increase of the energy density injected in the quench very similar to the $h > 0$ domain (starting with a quadratic rise and having a linear asymptotics for large $|h|$, cf. Fig. IV.2), this explains the rapid rise in $\bar{\partial}_t S$. Note that even though A_+ becomes unstable at h_- , it barely has any

effect on entropy generation. The reason is that the gap and Lieb-Robinson velocity of A_+ behave in an opposite way compared to A_- , so with h becoming more negative the share of A_+ in the entropy production decreases fast. By the time h passes through h_- , the only observable effect of A_+ becoming unstable is a hint of an inflection point in the dependence of $\overline{\partial_t S}$ on h at the threshold (cf. Fig. IV.4).

V. CONCLUSIONS AND OUTLOOK

In this work we considered quantum quenches in the paramagnetic phase of the quantum Potts spin chain corresponding to switching on a longitudinal magnetic field. We have demonstrated that the entanglement entropy production rate shows a deep relation with the quasi-particle spectrum. In particular, the mean entanglement

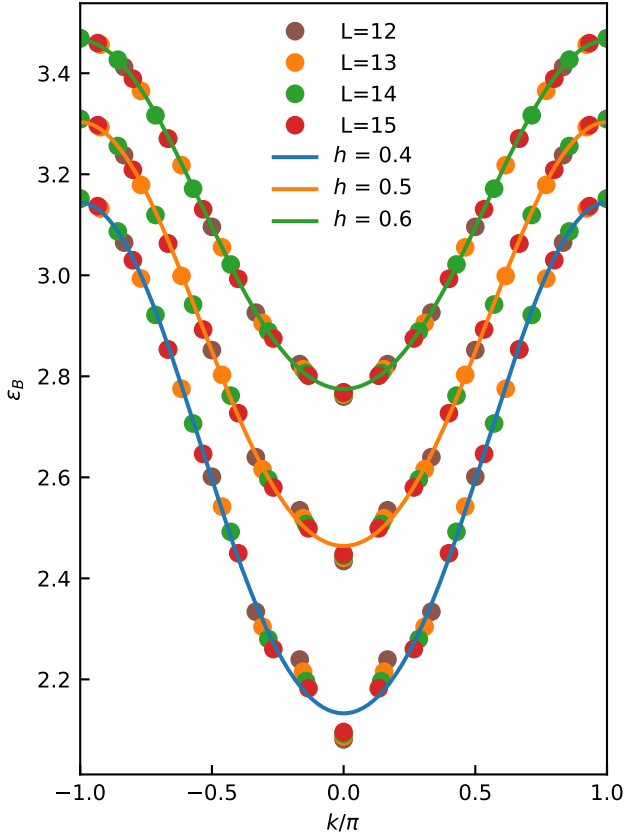


Figure III.6: Dispersion relation for B at $g = 1.5$ and $h = 0.4, 0.5$ and 0.6 . Energies are shown in units of J , while momentum is shown in units of $1/a$, where a is the lattice spacing.

entropy production rate $\overline{\partial_t S}$ is greatly enhanced by the appearance of a new quasi-particle species in the spectrum, which is a manifestation of Gibbs mixing entropy corresponding to species information. These findings are completely consistent with the results obtained for the Ising case in [47], showing the general nature of the effect and confirming its interpretation as a non-equilibrium manifestation of the so-called Gibbs paradox. We have also shown that for very large $h > 0$ the entropy production rate decreases towards zero, which can be understood from the freezing of spin chain dynamics.

In contrast with the Ising model, for the Potts case the domain $h < 0$ has a different physics since the spin dynamics does not freeze for any magnitude of h , and indeed in that domain we observed a monotonous increase of $\overline{\partial_t S}$ with $|h|$, the qualitative details of which again could be fully understood from the quasi-particle spectrum.

As we noted, a detailed quantitative description of the entanglement entropy production is not yet available. All the available evidence shows that the quenches considered here are of sufficiently small density to admit an essentially semi-classical quasi-particle description following the picture proposed by Calabrese and Cardy in

their seminal works [10, 12]. There has been substantial recent work aiming at extending the quasi-particle description beyond the simple picture of production of independent pairs, such as to cases with no pair structure [41], and initial states with correlated pairs [59].

The missing main ingredient is a suitable theoretical calculation of the quasi-particle production rates as functions of the quench parameter h . Once the amplitudes are available, one can try to develop a theory for the entanglement entropy production following the lines of [41]. Albeit in contrast to the case in [41] the system we consider has interacting quasi-particles, it seems likely that in the regime of transverse field g close enough to the critical value 1, the post-quench density is small enough so that effects of interactions between the quasi-particle do not affect substantially the post-quench time evolution once the particles were created and so the description would at least be semi-quantitative. The missing ingredient necessary for such a description is quantitative knowledge of quasi-particle creation rates as a function of the quench parameter h ; at this time, such information is only available for the Ising case and even there only in the scaling field theory limit [60].

Acknowledgments

This research was supported by the National Research Development and Innovation Office (NKFIH) under a K-2016 grant no. 119204, and also by the BME-Nanotechnology FIKP grant of EMMI (BME FIKP-NAT). G.T. was also supported by the Quantum Technology National Excellence Program (Project No. 2017-1.2.1-NKP-2017- 00001).

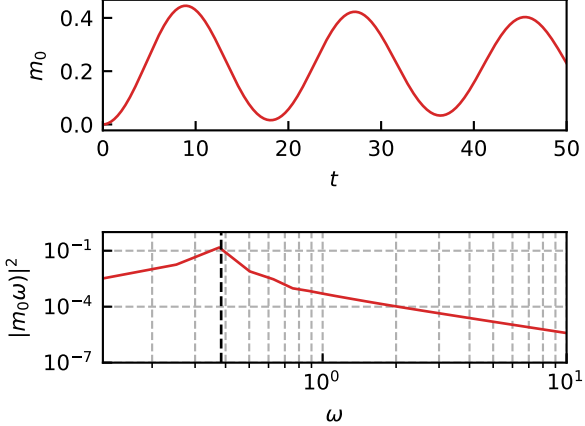
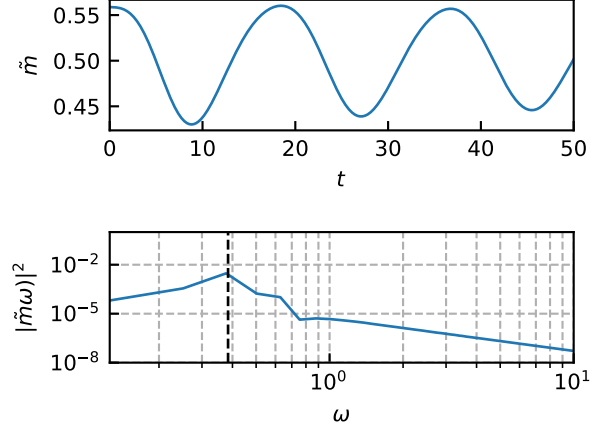
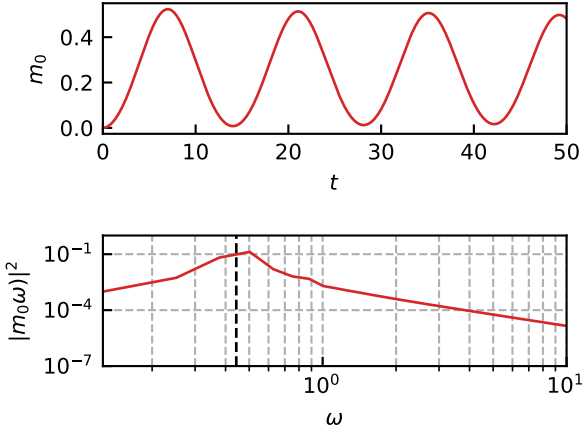
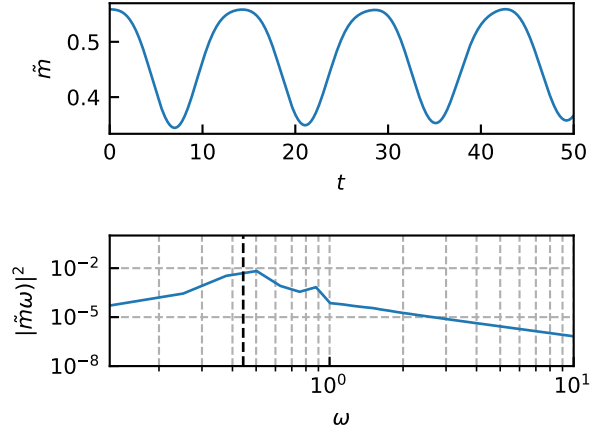
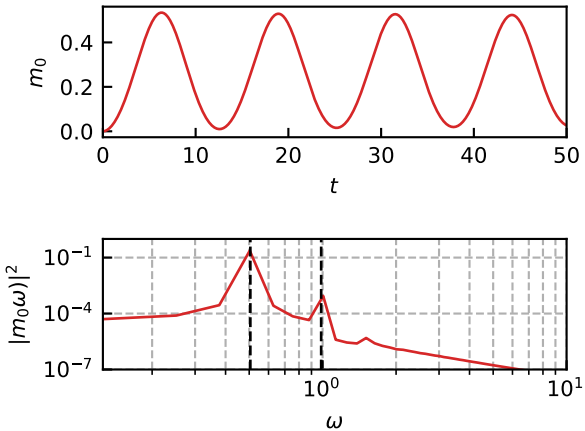
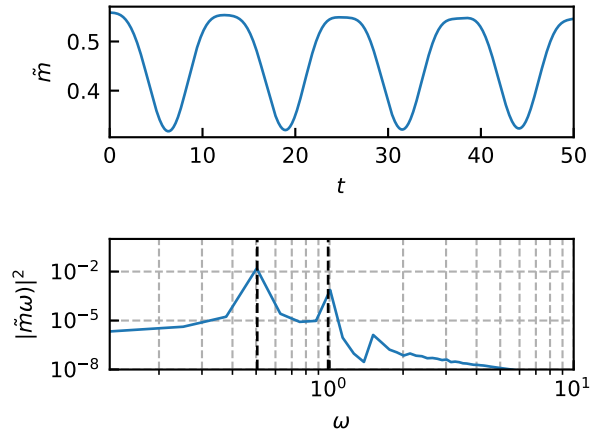
(a) $m_1(t)$ and its FPS for $h = 0.06$ (b) $\tilde{m}(t)$ and its FPS for $h = 0.06$ (c) $m_1(t)$ and its FPS for $h = 0.1$ (d) $\tilde{m}(t)$ and its FPS for $h = 0.1$ (e) $m_1(t)$ and its FPS for $h = 0.12$ (f) $\tilde{m}(t)$ and its FPS for $h = 0.12$

Figure IV.1: Time evolution of the longitudinal and transverse magnetisations $m_0(t)$ resp. $\tilde{m}(t)$ for $g = 1.25$ and $h = 0.06, 0.10$ and 0.12 , showing both the real time dependence and its Fourier power spectrum (FPS). Frequencies are shown in units of J .

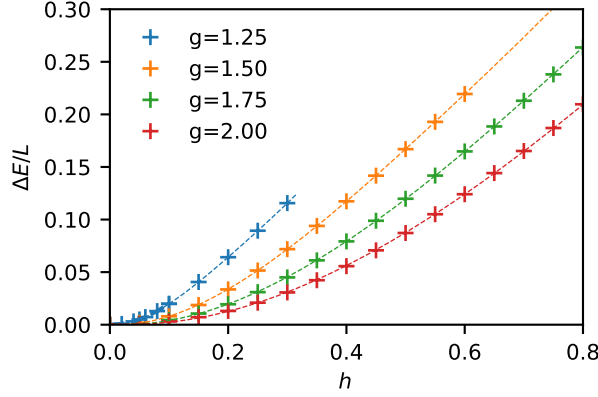


Figure IV.2: Density of energy (in units of J/a , with a denoting the lattice spacing) released by the quench as a function of h .

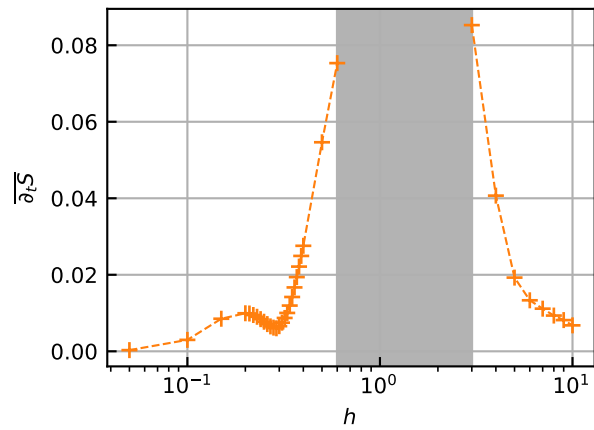


Figure IV.3: Entanglement entropy production rate $\overline{\partial_t S}$ for $g = 1.5$, including the regime of large $h > 0$. The shaded region corresponds to a parameter range where entropy growth was so fast that $\overline{\partial_t S}$ could not be evaluated from iTEBD as it was impossible to follow the dynamics for long enough times.

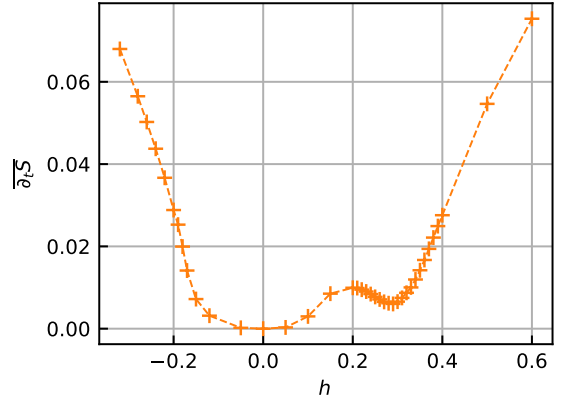


Figure IV.4: Entanglement entropy production rate $\overline{\partial_t S}$ for $g = 1.5$ including the range $h < 0$

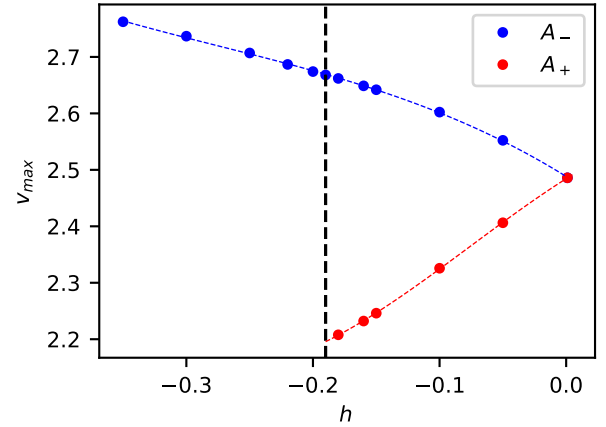
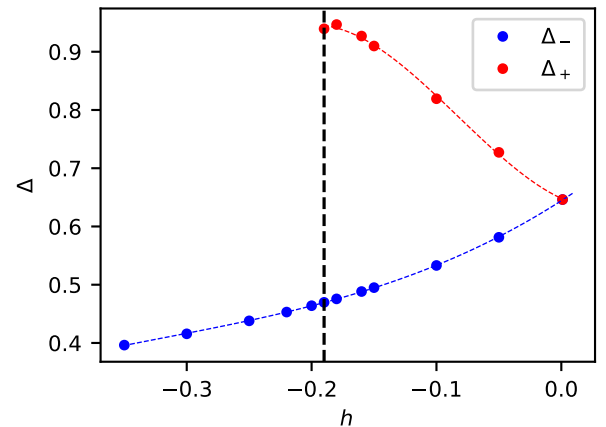


Figure IV.5: Quasi-particle gaps Δ_{\pm} (in units of J) and Lieb-Robinson velocities $v_{\max\pm}$ (in units of Ja , where a is the lattice spacing) for $h < 0$ (with $g = 1.5$). The vertical dashed line shows the threshold value $h_- \approx -0.19$ beyond which A_+ becomes unstable and decays into two A_- quasi-particles.

[1] M. Cheneau, P. Barmettler, D. Poletti, M. Endres, P. Schauss, T. Fukuhara, C. Gross, I. Bloch, C. Kollath, and S. Kuhr: Light-cone-like spreading of correlations in a quantum many-body system, *Nature* **481** (2012) 484-487.

[2] A. M. Kaufman, M. E. Tai, A. Lukin, M. Rispoli, R. Schittko, P. M. Preiss, and M. Greiner: Quantum thermalization through entanglement in an isolated many-body system, *Science* **353** (2016) 794-800.

[3] T. Kinoshita, T. Wenger and D. S. Weiss: A quantum Newton's cradle, *Nature* **440** (2006) 900-903.

[4] S. Hofferberth, I. Lesanovsky, B. Fischer, T. Schumm and J. Schmiedmayer: Non-equilibrium coherence dynamics in one-dimensional Bose gases, *Nature* **449** (2007) 324-327.

[5] S. Trotzky, Y.-A. Chen, A. Flesch, I. P. McCulloch, U. Schollwöck, J. Eisert and I. Bloch: Probing the relaxation towards equilibrium in an isolated strongly correlated 1D Bose gas, *Nature Phys.* **8** (2012) 325-330.

[6] T. Langen, S. Erne, R. Geiger, B. Rauer, T. Schweigler, M. Kuhnert, W. Rohringer, I. E. Mazets, T. Gasenzer and J. Schmiedmayer: Experimental observation of a generalized Gibbs ensemble, *Science* **348** (2015) 207-211.

[7] F. Meinert, M. J. Mark, E. Kirilov, K. Lauber, P. Weinmann, A. J. Daley and H.-C. Nägerl: Many-body quantum quench in an atomic one-dimensional Ising chain, *Phys. Rev. Lett.* **111** (2013) 053003.

[8] T. Fukuhara, P. Schauß, M. Endres, S. Hild, M. Cheneau, I. Bloch, and C. Gross: Microscopic observation of magnon bound states and their dynamics, *Nature* **502** (2013) 76-79.

[9] T. Langen, R. Geiger, M. Kuhnert, B. Rauer, and J. Schmiedmayer: Local emergence of thermal correlations in an isolated quantum many-body system, *Nature Phys.* **9** (2013) 640-643.

[10] P. Calabrese and J. Cardy: Time-dependence of correlation functions following a quantum quench, *Phys. Rev. Lett.* **96** (2006) 136801.

[11] E.H. Lieb and D.W. Robinson: The finite group velocity of quantum spin systems, *Commun. Math. Phys.* **28** (1972) 251-257.

[12] P. Calabrese and J. Cardy: Evolution of Entanglement Entropy in One-Dimensional Systems, *J. Stat. Mech.* **0504** (2005) P04010.

[13] M. Fagotti and P. Calabrese: Evolution of entanglement entropy following a quantum quench: Analytic results for the XY chain in a transverse magnetic field, *Phys. Rev. A* **78** (2008) 010306.

[14] V. Eisler and I. Peschel: Entanglement in a periodic quench, *Ann. Phys. (Berlin)* **17** (2008) 410-423.

[15] M. G. Nezhadaghghi and M. A. Rajabpour: Entanglement dynamics in short and long range harmonic oscillators, *Phys. Rev. B* **90** (2014) 205438 .

[16] M. Kormos, L. Bucciantini and P. Calabrese: Stationary entropies after a quench from excited states in the Ising chain, *EPL* **107** (2014) 40002; L. Bucciantini, M. Kormos, and P. Calabrese: Quantum quenches from excited states in the Ising chain, *J. Phys. A* **47** (2014) 175002.

[17] M. Collura, M. Kormos, and P. Calabrese: Stationary entropies following an interaction quench in 1D Bose gas, *J. Stat. Mech.* **1401** (2014) P01009.

[18] L. Hackl, E. Bianchi, R. Modak and M. Rigol, Entanglement production in bosonic systems: Linear and logarithmic growth, *Phys. Rev. A* **97** (2018) 032321.

[19] G. De Chiara, S. Montangero, P. Calabrese, and R. Fazio: Entanglement Entropy dynamics in Heisenberg chains, *J. Stat. Mech.* **0603** (2006) P03001.

[20] A. Laeuchli and C. Kollath: Spreading of correlations and entanglement after a quench in the Bose-Hubbard model, *J. Stat. Mech.* **0805** (2008) P05018.

[21] H. Kim and D. A. Huse: Ballistic Spreading of Entanglement in a Diffusive Nonintegrable System, *Phys. Rev. Lett.* **111** (2013) 127205.

[22] M. Fagotti and M. Collura: Universal prethermalisation dynamics of entanglement entropies after a global quench, arXiv:1507.02678.

[23] A. S. Buyskikh, M. Fagotti, J. Schachenmayer, F. Essler and A. J. Daley: Entanglement growth and correlation spreading with variable-range interactions in spin and fermionic tunnelling models, *Phys. Rev. A* **93** (2016) 053620; I. Frerot, P. Naldesi, and T. Roscilde: Multi-speed prethermalization in spin models with power-law decaying interactions, *Phys. Rev. Lett.* **120** (2018) 050401.

[24] J. Dubail, J.-M. Stephan, J. Viti and P. Calabrese: Conformal field theory for inhomogeneous one-dimensional quantum systems: the example of non-interacting Fermi gases, *SciPost Phys.* **2** (2017) 002.

[25] A. Coser, E. Tonni and P. Calabrese: Entanglement negativity after a global quantum quench, *J. Stat. Mech.* **1412** (2014) P12017.

[26] J. S. Cotler, M. P. Hertzberg, M. Mezei, and M. T. Mueller: Entanglement Growth after a Global Quench in Free Scalar Field Theory, *JHEP* **1611** (2016) 166.

[27] N. Schuch, M.M. Wolf, F. Verstraete and J.I. Cirac: Entropy Scaling and Simulability by Matrix Product States, *Phys. Rev. Lett.* **100** (2008) 030504; N. Schuch, M.M. Wolf, K. G. H. Vollbrecht, and J.I. Cirac: On entropy growth and the hardness of simulating time evolution, *New J. Phys.* **10** (2008) 033032.

[28] A. Perales and G. Vidal: Entanglement growth and simulation efficiency in one-dimensional quantum lattice systems, *Phys. Rev. A* **78** (2008) 042337.

[29] P. Hauke, F.M. Cucchietti, L. Tagliacozzo, I. Deutsch and M. Lewenstein: Can one trust quantum simulators?, *Rep. Prog. Phys.* **75** (2012) 082401.

[30] J. Dubail: Entanglement scaling of operators: a conformal field theory approach, with a glimpse of simulability of long-time dynamics in 1+1d, *J. Phys. A* **50** (2017) 234001.

[31] A. J. Daley, H. Pichler, J. Schachenmayer and P. Zoller, Measuring Entanglement Growth in Quench Dynamics of Bosons in an Optical Lattice, *Phys. Rev. Lett.* **109** (2012) 020505.

[32] R. Islam, R. Ma, P. M. Preiss, M. E. Tai, A. Lukin, M. Rispoli and M. Greiner: Measuring entanglement entropy in a quantum many-body system, *Nature* **528** (2015) 77-83.

[33] V. Alba and P. Calabrese: Entanglement and thermodynamics after a quantum quench in integrable systems, *PNAS* **114** (2017) 7947-7951.

[34] J. M. Deutsch, H. Li and A. Sharma: Microscopic origin of thermodynamic entropy in isolated systems, *Phys. Rev. E* **87** (2013) 042135.

[35] W. Beugeling, A. Andreanov and M. Haque: Global characteristics of all eigenstates of local many-body Hamiltonians: participation ratio and entanglement entropy, *J. Stat.*

Mech. **1502** (2015) P02002.

[36] V. Alba and P. Calabrese: Quench action and Rényi entropies in integrable systems, *Phys. Rev.* **B96** (2017) 115421; V. Alba and P. Calabrese: Rényi entropies after releasing the Néel state in the XXZ spin chain, *J. Stat. Mech.* **1711** (2017) 113105.

[37] V. Alba and P. Calabrese: Entanglement dynamics after quantum quenches in generic integrable systems, *SciPost Phys.* **4** (2018) 017.

[38] M. Mestyán, V. Alba and P. Calabrese: Rényi entropies of generic thermodynamic macrostates in integrable systems, *J. Stat. Mech.* **1808** (2018) 083104.

[39] P. Calabrese, F.H.L. Essler and M. Fagotti: Quantum Quench in the Transverse-Field Ising Chain, *Phys. Rev. Lett.* **106** (2011) 227203;
P. Calabrese, F.H.L. Essler and M. Fagotti: Transverse Field Ising chain I: Time evolution of order parameter correlators, *J. Stat. Mech.* **1207** (2012) P07016 ;
P. Calabrese, F.H.L. Essler and M. Fagotti: Quantum Quench in the Transverse Field Ising Chain II: Stationary State Properties, *J. Stat. Mech.* **1207** (2012) P07022.

[40] M. Kormos and G. Zaránd: Quantum quenches in the sine-Gordon model: a semiclassical approach, *Phys. Rev.* **E93** (2016) 062101;
C.P. Moca, M. Kormos and G. Zaránd: Semi-semiclassical theory of quantum quenches in one dimensional systems, *Phys. Rev. Lett.* **119** (2017) 100603.

[41] B. Bertini, E. Tartaglia and P. Calabrese: Entanglement and diagonal entropies after a quench with no pair structure, *J. Stat. Mech.* **1806** (2018) 063104.

[42] O. A. Castro-Alvaredo, B. Doyon and T. Yoshimura: Emergent hydrodynamics in integrable quantum systems out of equilibrium, *Phys. Rev.* **X6** (2016) 41065 .

[43] B. Bertini, M. Collura, J. De Nardis and M. Fagotti: Transport in Out-of-Equilibrium XXZ Chains: Exact Profiles of Charges and Currents, *Phys. Rev. Lett.* **117** (2016) 207201.

[44] B. Bertini, M. Fagotti, L. Piroli and P. Calabrese: Entanglement evolution and generalised hydrodynamics: non-interacting systems, *J. Phys. A51* (2018) 39LT01.

[45] V. Alba: Towards a Generalized Hydrodynamics description of Rényi entropies in integrable systems, arXiv:1807.01800 [cond-mat.stat-mech].

[46] M. Kormos, M. Collura, G. Takács and P. Calabrese: Real time confinement following a quantum quench to a non-integrable model, *Nature Phys.* **13** (2017) 246-249.

[47] M. Collura, M. Kormos and G. Takács: Dynamical manifestation of Gibbs paradox after a quantum quench, arXiv:1801.05817 [cond-mat.stat-mech].

[48] G. Vidal: Efficient Simulation of One-Dimensional Quantum Many-Body Systems, *Phys. Rev. Lett.* **93** (2004) 040502;
G. Vidal: Classical Simulation of Infinite-Size Quantum Lattice Systems in One Spatial Dimension, *Phys. Rev. Lett.* **98** (2007) 070201.

[49] Á. Rapp, P. Schmitteckert, G. Takács and G. Zaránd: Asymptotic scattering and duality in the one-dimensional three-state quantum Potts model on a lattice, *New Journal of Physics* **15** (2013) 013058.

[50] G. Delfino and P. Grinza: Confinement in the q-state Potts field theory, *Nucl. Phys.* **B791** (2008) 265–283.

[51] L. Lepori, G.Z. Tóth and G. Delfino: The particle spectrum of the three-state Potts field theory: a numerical study, *J. Stat. Mech.* **0911** (2009) P11007.

[52] S.B. Rutkevich: Two-kink bound states in the magnetically perturbed Potts field theory at $T < T_c$, *J. Phys.* **A43** (2010) 235004.

[53] S.B. Rutkevich: Baryon masses in the three-state Potts field theory in a weak magnetic field, *J. Stat. Mech.* **1501** (2015) P01010.

[54] M. Lencsés and G. Takács: Confinement in the q-state Potts model: an RG-TCSA study, *JHEP* **1509** (2015) 146.

[55] M. Lüscher: Volume dependence of the energy spectrum in massive quantum field theories. I. Stable particle states, *Commun. Math. Phys.* **104** (1986) 177-206.

[56] M. Lüscher: Volume dependence of the energy spectrum in massive quantum field theories. II. Scattering states, *Commun. Math. Phys.* **105** (1986) 153-188.

[57] A.B. Zamolodchikov: Ising Spectroscopy II: Particles and poles at $T > T_c$, arXiv:1310.4821 [hep-th].

[58] T. Rakovszky, M. Mestyán, M. Collura, M. Kormos and G. Takács: Hamiltonian truncation approach to quenches in the Ising field theory, *Nucl. Phys.* **B911** (2016) 805-845.

[59] A. Bastianello and P. Calabrese: Spreading of entanglement and correlations after a quench with intertwined quasiparticles, arXiv:1807.10176.

[60] K. Hódsági, M. Kormos and G. Takács: Quench dynamics of the Ising field theory in a magnetic field, *SciPost Phys.* **5** (2018) 027.